

## SUPPLEMENTAL MATERIAL ITEM S1

### Geology of the Grenville Province

The Grenville Province, once the orogenic core of the supercontinent Rodinia, is today exposed as a broad swath of rock stretching from northeastern Labrador, Canada southwest to eastern Ontario, as well as the Adirondack Mountains in New York, USA. Grenville rocks also form the basement of the younger Appalachian Mountains in the eastern USA, Nova Scotia, and Newfoundland, with numerous disconnected Grenville ‘inliers’ exposed through windows in younger rocks. In this section, we briefly review the geologic history and structure of the Grenville Province. Figure 11 in Hynes and Rivers (2010) is an excellent schematic tectonic cartoon, and Rivers (2015) provide a comprehensive review of the structural framework and litho-tectonic units with updated nomenclatures from the LITHOPROBE program.

The amalgamation of Rodinia is reflected by a series of orogenic events in Laurentia: the accretionary Elzevirian orogeny (1245-1220 Ma), the arc-collisional Shawinigan orogeny (1190-1140 Ma), and finally the continent-continent collisional Grenville orogeny (1090-980 Ma) that is subdivided into Ottawa (1090-1020 Ma) and Rigolet (1015-980 Ma) stages (Rivers, 2012; Chiarenzelli et al., 2010; Indares, 2020). In older nomenclatures, Shawinigan was also a part of the Grenville cycle. Prior to the start of “Grenvillian” orogenesis, the southeastern juvenile margin of Laurentia consisted of long-lived continental arcs and small accreted island-arc terranes, with subduction directed to the northwest. Two of the most significant continental arc systems were the Labradorian (1710-1650 Ma) and Pinwarian (1510-1405 Ma) (Gower et al., 2008). Peri-Laurentian island arcs and the associated back-arc basins were active until ~1.30 Ga. The Elzevirian orogeny involved the initiation of back-arc basin closure, docking of arc terranes, and a switch to SE-directed subduction (Hynes and Rivers, 2010; McLelland et al., 2013). SE-directed subduction fueled continuing island arc activity, partially built on rifted Laurentian margin. Shawinigan orogeny began with the accretion of two arc belts: The Composite Arc Belt (CAB), underlain by oceanic crust and exposed in eastern Ontario and southern Quebec, and the Frontenac-Adirondack Arc Belt (FAB), built on Laurentian platform and consisting of easternmost Ontario, southeastern Quebec, and the Adirondack Highlands and Lowlands (Hynes and Rivers, 2010). Following arc accretion was a rapid transition to anorogenic magmatism (Chiarenzelli et al., 2010). The protracted Shawinigan magmatic flare-up was widespread from Newfoundland to Texas, overprinting just-accreted arc terranes. A major magmatic pulse of predominantly anorthosite-mangerite-charnockite-granite (AMCG) plutons occurred between approximately 1180 Ma and 1130 Ma, with AMCG massifs emplaced throughout the Laurentian margin in a broad region of extension (McLelland et al., 2013). AMCG complexes were conventionally

associated with mantle-derived magmas, but recent geochemical studies suggest that at least limited crustal contamination was involved (e.g., Peck, 2010).

Crustal shortening resumed around 1090 Ma, culminating in the continental collision between Laurentia and Amazonia during the Ottawa stage (Rivers, 2012). A suture between the two cratons is inferred within the Appalachian Blue Ridge Province based on contrasting model ages (Johnson et al., 2020). The Allochthon Boundary Thrust (ABT), the largest shear zone of the Grenville Province, formed at the base of the Grenville hinterland during the earliest Ottawa stage and accommodated at least 100 km of crustal shortening (Hynes and Rivers, 2010). The ABT separates the Parautochthonous Belt from allochthon terranes. The majority of the contiguous Grenville hinterland southeast of the ABT yields Ottawa metamorphic ages, overprinting earlier Shawinigan and Elzevirian metamorphism in parts of the CAB and FAB (Hynes and Rivers, 2010). These shear-zone-bounded terranes are grouped into the Low-, Medium-, and High-Pressure Belts, exhibiting upper-amphibolite to granulite facies, granulite facies, and granulite with local eclogite facies, respectively. The deepest-seat rocks crop out in the western Grenville in Ontario (Rivers et al., 2002), where eclogites along ABT yield early Ottawa (~1090 Ma; Marsh and Culshaw, 2014) metamorphic ages and underwent granulite- to amphibolite-facies overprinting. In contrast, the high-P counterpart in central Grenville was metamorphosed during mid- to late-Ottawa (Indares, 2020). The Adirondack Highlands and the Lowlands were both subject to intense metamorphism during the Shawinigan orogeny, but only the Adirondack Highlands were overprinted by high-grade Ottawa-age metamorphism. The numerous Appalachian Grenville inliers broadly experienced the same tectonomagmatic phases as the northern contiguous Grenville Province (Rivers, 2012; McLelland et al., 2013).

Magmatism in the early- to mid-Ottawa consisted of A-type and AMCG plutonism (Morisset et al., 2009; Groulier et al., 2018) and was spatially limited to areas approximately 150 km south of the ABT (Rivers and Hynes, 2010). High-grade metamorphism and widespread anatexis in the early- to mid-Ottawa stage gave way to syn- to post-tectonic extension in the mid- to late-Ottawa (Rivers, 2012). The late Ottawa stage involved a second, weaker metamorphic pulse between 1040 Ma and 1020 Ma and an extensional re-working of the ABT around 1020 Ma (Rivers, 2012; Indares, 2020).

The Rigolet stage of the Grenville orogeny occurred following a brief pause in metamorphism and post-orogenic gravitational collapse at the end of Ottawa. Propagation of the orogen westward into the former Ottawa foreland created the Grenville Front, which became the site of renewed crustal shortening (Hynes and Rivers, 2010). The Parautochthonous Belt, located between northwest of the ABT on the hanging wall of the Grenville Front, forms a fold-and-thrust belt with SE-dipping fabrics and yields Rigolet metamorphic ages. The intensity of metamorphism increases from the Grenville Front to the west from greenschist to upper amphibolite-facies conditions. Areas lacking Grenville-age

metamorphism (the 'orogenic lid') occur in regions of the CAB and FAB, and along the ABT in northeastern Quebec and southern Labrador (Indares, 2020). The Rigolet stage was followed by orogenic collapse of the Grenville hinterland in a basin-and-range system (Hynes and Rivers, 2010; Rivers, 2012; Groulier et al., 2018).

## References

- Chiarenzelli, J., Selleck, B., Lupulescu, M., Regan, S., Bickford, M. E., Valley, P., McLelland, J., and York, N., 2017, Lyon Mountain ferroan leucogranite suite: Magmatic response to extensional thinning of overthickened crust in the core of the Grenville orogen: *GSA Bulletin*, v. 129, no. 11/12, p. 1472–1488, doi: 10.1130/B31697.1.
- Hynes, A., and Rivers, T., 2010, Protracted continental collision – evidence from the Grenville Orogen: *Canadian Journal of Earth Science*, v. 47, p. 591-620, doi:10.1139/E10-003.
- Indares, A., 2020, Deciphering the metamorphic architecture and magmatic patterns of large hot orogens: Insights from the central Grenville Province: *Gondwana Research*, v. 80, p. 385-409, doi:10.1016/j.gr.2019.10.013.
- Johnson, T. A., Mulcahy, S. R., Vervoort, J. D., Ramsey, M. J., and Southworth, S., 2020, Tectonic evolution of the Grenville Orogen in the central Appalachians: *Precambrian Research*, v. 34, no. 105740, p. 1-21, doi:10.1016/j.precamres.2020.105740.
- Marsh, J.H. and Culshaw, N.G., 2014. Timing and conditions of high-pressure metamorphism in the western Grenville Province: constraints from accessory mineral composition and phase equilibrium modeling. *Lithos*, v. 200, p. 402-417, doi: 10.1016/j.lithos.2014.04.016
- McLelland, J. M., Selleck, B. W., and Bickford, M. E., 2013, Tectonic Evolution of the Adirondack Mountains and Grenville Orogen Inliers within the USA: *Geoscience Canada*, v. 40, no. 4, p. 318-352, doi:10.12789/geocanj.2013.40.022.
- Morisset, C.-E., Scoates, J. S., Weis, D., and Friedman, R. M., 2009, U-Pb and  $^{40}\text{Ar}/^{39}\text{Ar}$  geochronology of the Saint-Urbain and Lac Allard (Havre-Saint-Pierre) anorthosites and their associated Fe-Ti oxide ores, Québec: Evidence for emplacement and slow cooling during the collisional Ottawa orogeny in the Grenville Province: *Precambrian Research*, v. 174, no. 1-2, p. 95-116, doi:10.1016/j.precamres.2009.06.009.
- Peck, W.H., Clechenko, C.C., Hamilton, M.A. and Valley, J.W., 2010. Oxygen isotopes in the Grenville and Nain AMCG suites: Regional aspects of the crustal component in massif anorthosites. *The Canadian Mineralogist*, v. 48(4), p.763-786, doi: 10.3749/canmin.48.4.763

- Rivers, T., 2008, Assembly and preservation of lower, mid, and upper orogenic crust in the Grenville Province – Implications for the evolution of large hot long-duration orogens: *Precambrian Research*, v. 167, p. 237-259, doi:10.1016/j.precamres.2008.08.005.
- Rivers, T., 2012, Upper-crustal orogenic lid and mid-crustal core complexes: signature of a collapsed orogenic plateau in the hinterland of the Grenville Province: *Canadian Journal of Earth Sciences*, v. 42, p. 1-42. doi:10.1139/E11-014.
- Rivers, T., 2015, Tectonic setting and evolution of the Grenville orogen: an assessment of progress over the last 40 years: *Geoscience Canada*, v. 42, p. 77-124, doi:10.12789/geocanj.2014.41.057.
- Gower, C.F., Kamo, S.L., Kwok, K., Krogh, T.E., 2008. Proterozoic southward accretion and Grenvillian orogenesis in the interior Grenville Province in eastern Labrador: evidence from U–Pb geochronological investigations. *Precambrian Research*, v. 165, p. 61–95, doi: 10.1016/j.precamres.2008.06.007

## SUPPLEMENTAL MATERIAL ITEM S2

### LA-ICP-MS analyses on Zircon Grains

Zircon grains were extracted by standard heavy liquid and magnetic techniques and then handpicked under a binocular microscope. The zircon grains, together with standards Qinghu (Li et al., 2013), were mounted in epoxy resin and then polished until the grain centers were exposed. The mount was vacuum-coated with high-purity gold before analysis. Reflected light and transmitted micrographs, as well as cathodoluminescence (CL) images, were performed to reveal each zircon's internal structures that help to choose suitable spot locations for U-Pb analyses. Larger zircons exhibiting igneous oscillatory zonation were chosen, and spots were selected to avoid metamorphic/alteration rims, large cracks, inclusions, and inherited cores. 100-150 out of the 250 zircons per sample were selected for U-Pb dating. Of those, the zircons of Grenvillian age (1.3-1.0 Ga) were analyzed for trace element content. The zircons were analyzed for in-situ U-Pb isotopes and trace elements using an NWR 193nm excimer laser ablation system coupled to an Agilent 7900 quadrupole ICP-MS at the University of Toronto.

#### *U-Pb dating*

The ICP-MS was tuned to achieve 100,000 counts per second sensitivity on  $^{206}\text{Pb}$  and  $< 3\%$  ThO/Th in NIST 610 standard with a 25  $\mu\text{m}$  spot size, 5 Hz repetition rate, and  $\sim 4.5 \text{ J/cm}^2$  laser fluence.

The analyses were conducted under the same instrumental conditions. Before the analysis, the samples were pre-ablated with 30  $\mu\text{m}$ , 5 Hz, and 5  $\text{J/cm}^2$  for 1 s to clean the surface of the grains. A 10 s wash-out followed the pre-ablation. Each analysis included 10 s background acquisition (laser warm-up) followed by 25 s laser ablation and 10 s wash-out. The following isotopes were measured, with dwell times:  $^{88}\text{Sr}$  (0.01s),  $^{206}\text{Pb}$  (0.03s),  $^{207}\text{Pb}$  (0.07s),  $^{208}\text{Pb}$  (0.01s) and  $^{238}\text{U}$  (0.02s).  $^{88}\text{Sr}$  was measured to monitor altered zircon and/or non-zircon grains.

For the external (primary) and monitor (secondary) zircon standards, we used in-house zircon standards DD91-1 and DD85-17. DD91-1 zircon is from the Lac Fournière pluton, a monzodiorite from northern Quebec, Canada dated at  $2682.4 \pm 1.0 \text{ Ma}$  ( $2\sigma$ , Davis, 2002). Zircon DD85-17 is from a quartz diorite from the Marmion batholith in northwest Ontario dated at  $3002 \text{ Ma} \pm 2.0 \text{ Ma}$  ( $2\sigma$ , Tomlinson et al., 2003). We used DD85-17 as the external (primary) standard for sample XC0-1 and XC0-3, and DD91-1 as the external standard for samples XC0-5, -6, -7, -8. For samples XC0-5, -6, -7, and -8, we also included zircon DD85-17 to monitor the accuracy of Pb/Pb and Pb/U ratios as a secondary standard. Each set of 4-6 analyses of sample zircons was bracketed by analyses of the external standard. One analysis of the monitor zircon was included for every 10 analyses of the sample zircons.

An in-house Excel-Visual Basic program developed by Dr. Don Davis was used for data reduction. For each analysis, the average background intensities for Pb and U isotopes were subtracted from sample intensities. Background subtracted isotopic ratios were then corrected for instrumental mass bias by normalizing to the reference values of zircon DD91-1 or DD85-17. Differences between standards were time-interpolated to correct sample measurements. Externally calibrated Pb/Pb and Pb/U ratios are reported. Analytical uncertainties in isotopic ratios for individual analyses are reported at the 68.3% confidence interval ( $1\sigma$ ). Systematic uncertainties are not included here, which include uncertainties in decay constants for  $^{238}\text{U}$  (0.16%) and  $^{235}\text{U}$  (0.21%) (Jaffey, 1971), and average uncertainty in external calibration. These systematic errors are around 1% ( $1\sigma$ ) Pb/Pb ratios, which are used to calculate ages but at least several percent for Pb/U ratios. Quoted uncertainties reflect counting errors only. Th/U ratios are calculated based on measured  $^{208}\text{Pb}/^{206}\text{Pb}$  ratios and  $^{207}\text{Pb}/^{206}\text{Pb}$  ages, assuming all  $^{208}\text{Pb}$  and  $^{206}\text{Pb}$  are radiogenic products from  $^{232}\text{Th}$  and  $^{238}\text{U}$ .

### ***Trace elements***

The ICP-MS was tuned to achieve 800,000 cps sensitivity on  $^{115}\text{In}$  in NIST-610 with a 25  $\mu\text{m}$  spot size, 10 Hz repetition rate, and  $\sim 6.2 \text{ J/cm}^2$  laser fluence. The oxidation rate was monitored using the ThO/Th ratios of the external standard and was maintained below 0.7% during the analyses.

$^{29}\text{Si}$ ,  $^{31}\text{P}$ ,  $^{44}\text{Ca}$ ,  $^{45}\text{Sc}$ ,  $^{49}\text{Ti}$ ,  $^{89}\text{Y}$ ,  $^{93}\text{Nb}$ ,  $^{139}\text{La}$ ,  $^{140}\text{Ce}$ ,  $^{141}\text{Pr}$ ,  $^{146}\text{Nd}$ ,  $^{147}\text{Sm}$ ,  $^{151}\text{Eu}$ ,  $^{153}\text{Eu}$ ,  $^{157}\text{Gd}$ ,  $^{159}\text{Tb}$ ,  $^{163}\text{Dy}$ ,  $^{165}\text{Ho}$ ,  $^{166}\text{Er}$ ,  $^{169}\text{Tm}$ ,  $^{172}\text{Yb}$ ,  $^{175}\text{Lu}$ ,  $^{178}\text{Hf}$ ,  $^{181}\text{Ta}$ ,  $^{208}\text{Pb}$ ,  $^{232}\text{Th}$ , and  $^{238}\text{U}$  were analyzed, all under the same instrumental conditions. Dwell time was set at 0.01s for  $^{29}\text{Si}$  and 0.05s for the other isotopes. Both  $^{151}\text{Eu}$  and  $^{153}\text{Eu}$  were analyzed to monitor interference from Ba oxides. We found no potential BaO interference on Eu in our analyzed samples. Total data acquisition for each sample was  $\sim 90\text{s}$ , including a 25s background acquisition before firing the laser, followed by 65 s of sample acquisition during ablation. NIST-610 were used as external standards, analyzed twice at the beginning and end of each analytical session ( $\sim 16$  unknowns). Qinghu zircons (Li et al., 2013) were analyzed for monitoring. The analyzed Qinghu REE patterns agree well with reported patterns (Fig. S1).

Sills data reduction software (Guillong et al., 2008) was used to correct for background, drift, instrumental bias and convert raw data to concentrations.  $^{29}\text{Si}$  was used as the internal standard.

### ***Data analysis***

We added previously published geochronology and trace element data to our analysis from another 125 Grenville-aged detrital zircons collected from the Kentucky ( $n = 59$ ) and St. Lawrence ( $n = 76$ ) rivers, respectively (Zhu et al., 2020). For these zircons, Gd was not reported, so the Gd concentrations were estimated by interpolation from the other trace elements (Tang et al., 2021b). Zircon

and whole-rock trace element data were normalized to the chondrite (Sun & McDonough, 1989). To calculate crustal thickness from [La/Yb] and [Eu/Eu\*], respectively, we used equations from Profeta et al., 2015, and Tang et al., 2021a, respectively:

$$d_m = 21.277 \ln(1.0204 \times [\text{La/Yb}]_N) \quad (1)$$

$$d_m = (84.2 \pm 9.2) \times [\text{Eu/Eu}^*]_{\text{zircon}} + (24.5 \pm 3.3) \quad (2)$$

Where  $d_m$  is crustal thickness (depth to Moho). The compilations of whole-rock chemistry and zircon data are provided in Data Repository Files DR3 and DR4.

The [Eu/Eu\*] proxy was calibrated against I-type intermediate and felsic intrusions, with SiO<sub>2</sub> between 55 and 75 wt.% in the Gangdese arc (Tang et al., 2021a). In this study, we compile the geochemical data in the same SiO<sub>2</sub> range. Although the [La/Yb] proxy was calibrated for intermediate arc magmatism (SiO<sub>2</sub> = 55-68 wt.%; Profeta et al., 2015), the application to felsic rocks does not show strong correlation between  $d_m$  and SiO<sub>2</sub> contents (Fig. S2). The pluton suite that show significant discrepancy between intermediate and felsic members is excluded (Mount Eve Granite; 1020 Ma; A-type).

The time sequence of whole-rock La/Yb and zircon Eu/Eu\* proxies underwent bootstrap resampling at  $\pm 35$  m.y. and  $\pm 25$  m.y. brackets, respectively. The bootstrapped moving averages of crustal thickness were generated using Acycle software (Li et al., 2019). The larger the bracket is, the smoother the fitted time-series trend becomes (Figs S4 & S5). Given that the total number of bulk-rock data is about 1.5 times of zircon data,  $\pm 35$  m.y bracket for the bulk-rock resampling creates a trend of similar smoothness as  $\pm 25$  m.y bracket for zircon. Thus, we use these two brackets to produce first-order trends with noises largely filtered.

**Table S1. Locations and source rivers for collected detrital zircons**

<b>Sample No.</b>	<b>Latitude</b>	<b>Longitude</b>	<b>River</b>
1	46.254310	-78.920381	Amable du Fond
2	46.320430	-78.709397	Ottawa
3	46.182317	-77.774027	Ottawa
4	45.903277	-77.279862	Petawawa
5	45.723471	-76.748571	Ottawa
6	45.467250	-76.404891	Ottawa
7	45.442416	-76.348780	Mississippi
8	45.408766	-75.923689	Ottawa

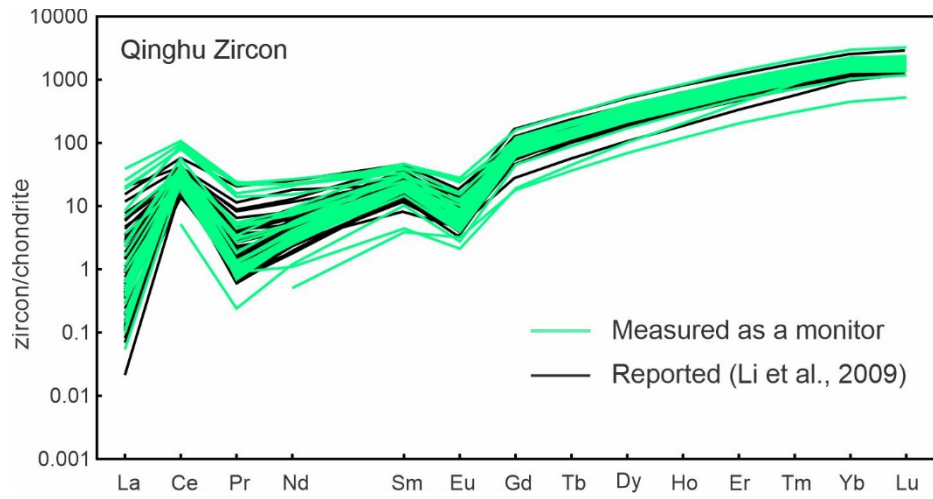


**Figure S1.** Comparison of chondrite-normalized REE patterns in analyzed Qinghu zircons and data reported in Li et al., 2009.

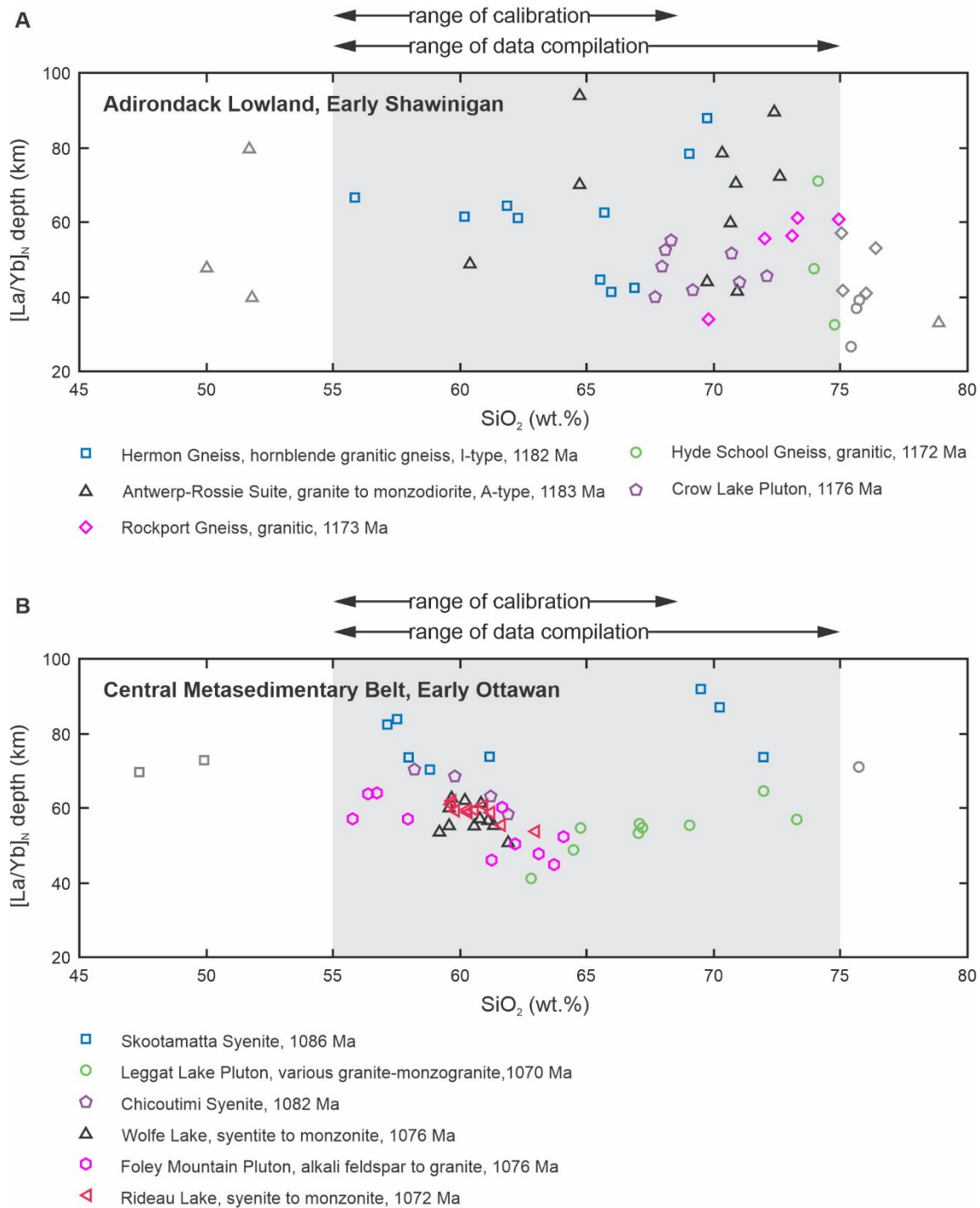


**Figure S2** Representative plots of the crustal depths derived from bulk-rock  $[La/Yb]_N$  proxy vs.  $SiO_2$  contents (wt.%) during collisional phases: (a) the early Shawinigan plutons in the Adirondack Lowlands and (b) early Ottawan plutons in the central Metasedimentary Belt. The grey symbols denote data excluded, and the shaded range is intermediate-felsic.

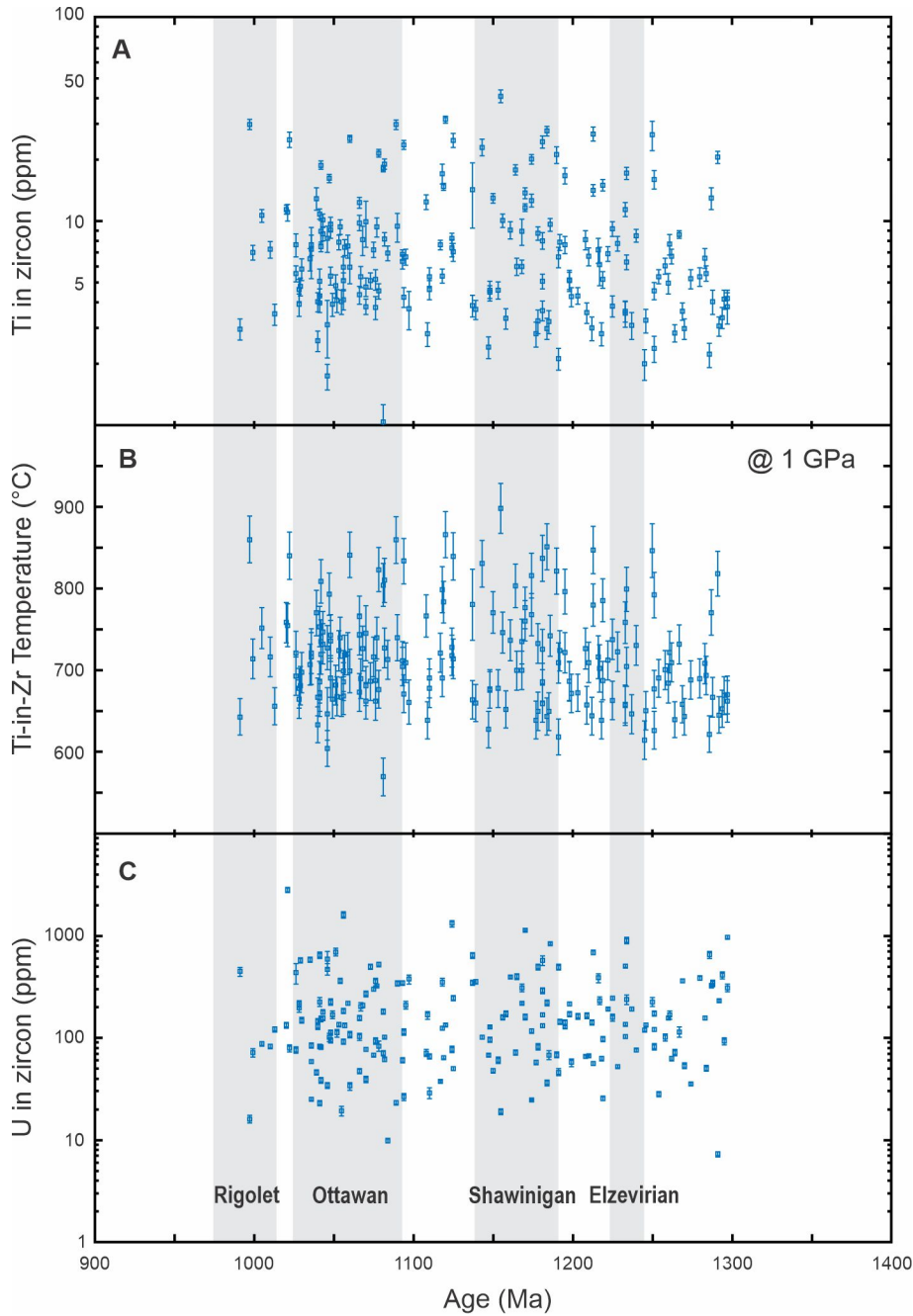


**Figure S3.** Compilation of Ti (a) and U (c) contents of zircon grains (unfiltered). The Ti-in-Zr temperatures (b) are calculated assuming unit  $\text{SiO}_2$  and  $\text{TiO}_2$  activities and using the thermometer calibrated by Ferry and Watson (2007). If the  $\text{SiO}_2$  activity is 0.9 and  $\text{TiO}_2$  activity is 0.5, typical for granitic system (e.g., Schiller and Finger, 2019), the temperature is overestimated by about 50 °C at 750 °C. The uncertainty is comparable to that from model parameters (errorbars). The errorbars on ages are omitted for a clear presentation.

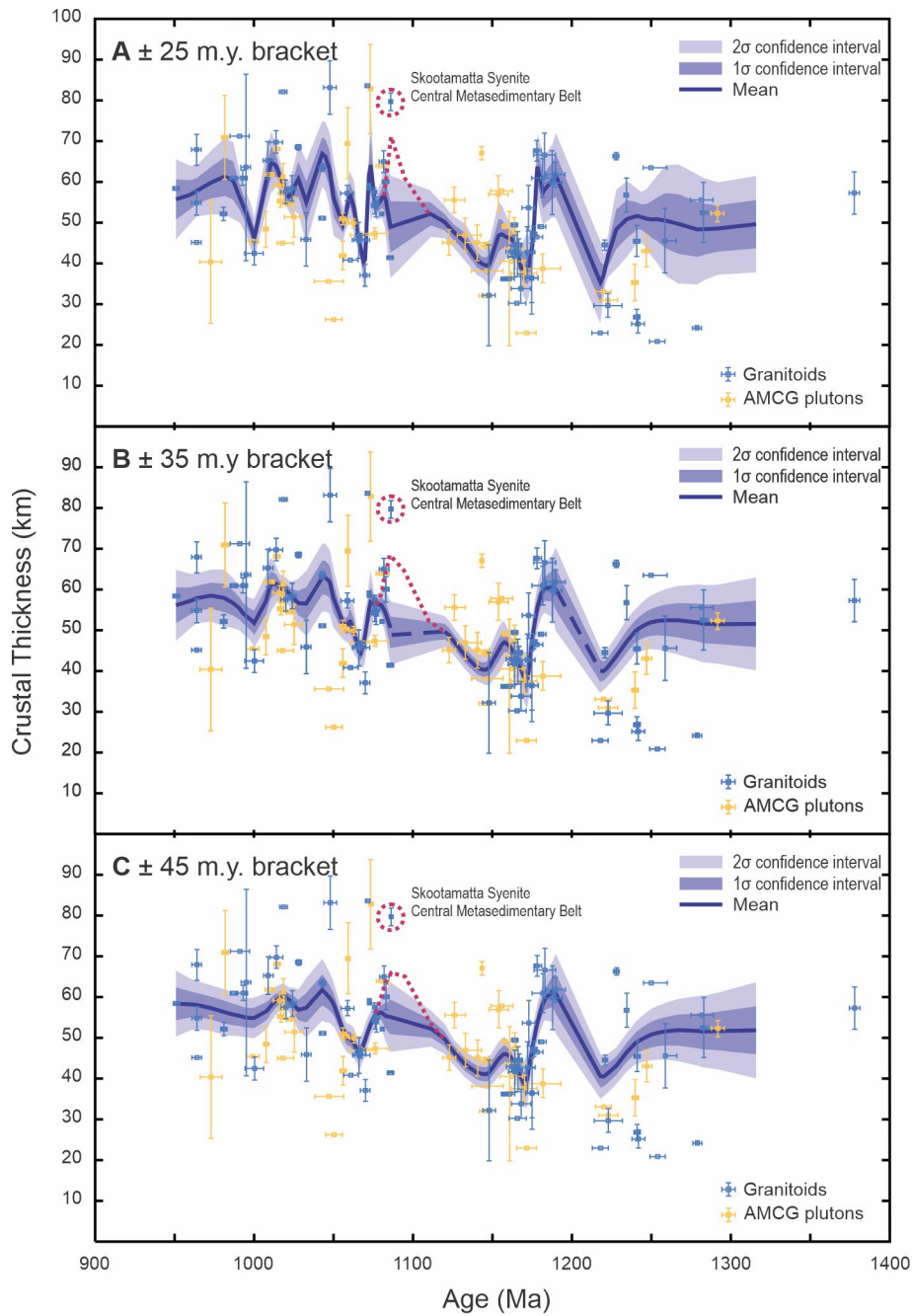


**Figure S4.** Crustal thickness trends based on whole-rock  $[La/Yb]_N$ , fitted by bootstrap with (a)  $\pm 25$ , (b)  $\pm 35$  and (c)  $\pm 45$  m.y. windows.  $1\sigma$  and  $2\sigma$  confidence intervals are shown as blue ribbons.

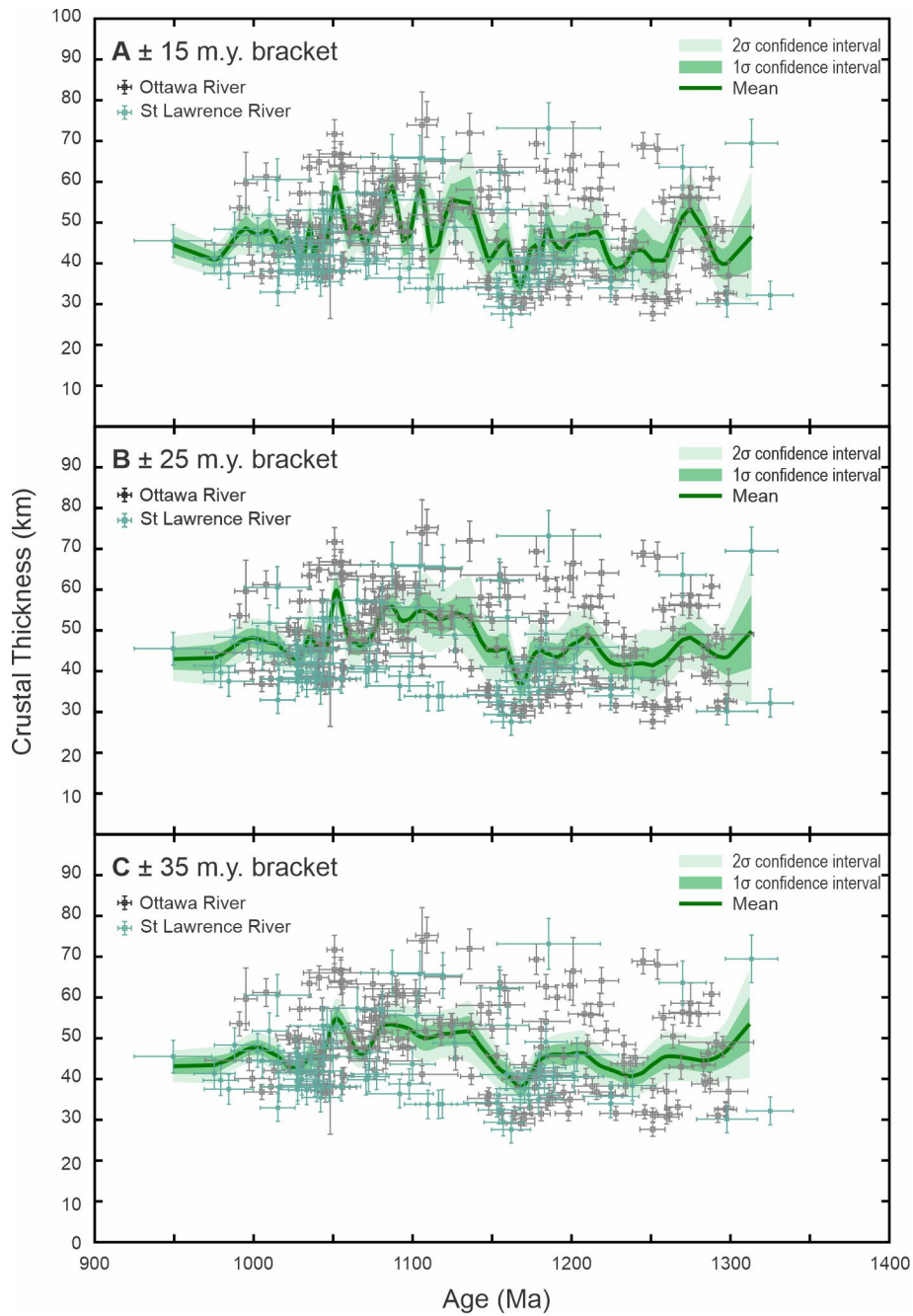


**Figure S5.** Crustal thickness trends based on zircon  $[Eu^*/Eu]$ , fitted by bootstrap with (a)  $\pm 15$ , (b)  $\pm 25$  and (c)  $\pm 35$  m.y. windows.  $1\sigma$  and  $2\sigma$  confidence intervals are shown as green ribbons.

## REFERENCES

- Davis, D.W., 2002. U–Pb geochronology of Archean metasedimentary rocks in the Pontiac and Abitibi subprovinces, Quebec, constraints on timing, provenance and regional tectonics. *Precambrian Research*, v. 115, p. 97–117, [https://doi.org/10.1016/S0301-9268\(02\)00007-4](https://doi.org/10.1016/S0301-9268(02)00007-4).
- Davis, D.W., and Sutcliffe, C.N., 2019. U-Pb Geochronology of Zircon and Monazite by LA-ICPMS in Samples from Northern Quebec. Quebec Ministry of Energy and Natural Resources, MB 2019-01.
- Ferry, J.M. and Watson, E.B., 2007. New thermodynamic models and revised calibrations for the Ti-in-zircon and Zr-in-rutile thermometers. *Contributions to Mineralogy and Petrology*, v. 154(4), p. 429-437, <https://doi.org/10.1007/s00410-007-0201-0>.
- Guillong, M., Meier, D.L., Allan, M.M., Heinrich, C.A., and Yardley, B.W.D., 2008. SILLS: A MATLAB-based program for the reduction of laser ablation ICP-MS data of homogeneous materials and inclusions. Mineralogical Association of Canada. Short Course. 40.
- Jaffey, A.H., Flynn, K.F., Glendenin, L.E., & Bentley, W.C., and Essling, A.M., 1971. Precisioun measurement of half-lives and specific activities of  $^{235}\text{U}$  and  $^{238}\text{U}$ . *Physical Review C*, v. 4, p. 1889-1906.
- Li, X., Gong, B., Yang, Y., and Hou, K., 2013. Qinghu zircon: A working reference for microbeam analysis of U-Pb age and Hf and O isotopes. *Chinese Science Bulletin*, v. 58, p. 4647–4654. <https://doi.org/10.1007/s11434-013-5932-x>
- Li, M., Hinnov, L. and Kump, L., 2019. Acycle: Time-series analysis software for paleoclimate research and education. *Computers & Geosciences*, v. 127, pp.12-22. <https://doi.org/10.1016/j.cageo.2019.02.011>
- Profeta, L., Ducea, M.N., Chapman, J. B., Paterson, S. R., Gonzales, S. M. H., Kirsch, M., Petrescu, L., & DeCelles, P. G. (2015). Quantifying crustal thickness over time in magmatic arcs. *Scientific Reports*, 5, 1–7. <https://doi.org/10.1038/srep17786>
- Schiller, D., and Finger, F. 2019. Application of Ti-in-zircon thermometry to granite studies: problems and possible solutions. *Contributions to Mineralogy and Petrology*, v. 174, p. 1-16, <https://doi.org/10.1007/s00410-019-1585-3>
- Sun, S.S., and McDonough, W.F., 1989. Chemical and isotopic systematics of oceanic basalts: Implications for mantle composition and processes. *Geological Society Special Publication*, v. 42, p. 313–345. <https://doi.org/10.1144/GSL.SP.1989.042.01.19>
- Tang, M., Ji, W., Chu, X., Wu, A., and Chen, C. 2021a. Reconstructing crustal thickness evolution from europium anomalies in detrital zircons. *Geology*, v. 49, p. 76–80. <https://doi.org/10.1130/G47745.1/5144012/g47745>
- Tang, M., Chu, X., Hao, J., and Shen, B. 2021b. Orogenic quiescence in Earth’s middle age. *Science*, v. 371, p. 728-731. <https://doi.org/10.1144/10.1126/science.abf1876>
- Tomlinson, K.Y., Davis, D.W., Stone, D. and Hart, T.R., 2003. U-Pb age and Nd isotopic evidence for crustal recycling and Archean terrane development in the south-central Wabigoon subprovince, Canada. *Contributions to Mineralogy and Petrology*, v. 144, p. 684-702. <https://doi.org/10.1007/s00410-002-0423-0>.